THE JOURNAL OF PHYSICAL CHEMISTRY C
A JOURNAL OF THE AMERICAN CHEMICAL SOCIETY

pubs.acs.org/JPCC

Article

Vibrational Energy Flow in Molecules Attached to Plasmonic Nanoparticles

Humanath Poudel, Pathick Halder Shaon, and David M. Leitner*

Cite This: https://doi.org/10.1021/acs.jpcc.4c01873

Read Online

ACCESS | Metrics & More | Article Recommendations | Supporting Information

ABSTRACT: The ability to control chemical reactions involving molecules attached to plasmonic nanoparticles requires information about vibrational energy flow. We compute the energy flow quantum mechanically in 5 substituted benzenethiols, including 4-nitrobenzenethiol (NBT), attached to plasmonic nanoparticles as well as rates of energy transfer to the surroundings. The lifetimes computed for Raman-active modes match those measured experimentally and are found to mainly result from intramolecular vibrational energy redistribution. Variation in lifetimes among the molecules arises from the tuning of resonances via different chemical groups. The lifetime of the NO stretch of NBT, which when excited can facilitate reaction, is computed to be close to the measured value and depends largely on resonances involving 3 other modes. We find that, upon comparison with the results of recent picosecond time-resolved measurements, the plasmonic resonance transfers energy to an excited electronic state, followed by rapid internal conversion to the ground state and vibrational cooling.

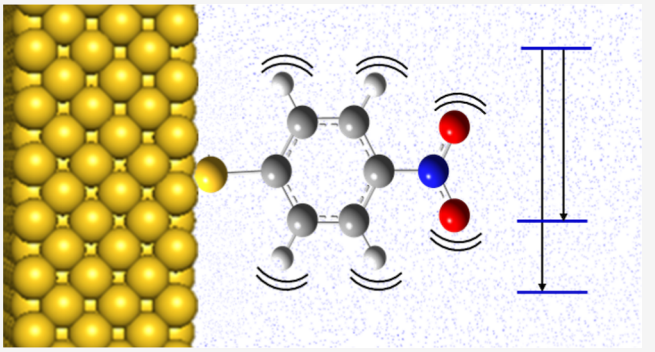

1. INTRODUCTION

The ability to facilitate chemical reactions via interactions between light and molecules attached to or near metal nanoparticles has motivated many studies of photochemical and photophysical processes in these systems.[1−14] Plasmonic nanoparticles catalyze, e.g., dimerization, dissociation, and reduction of chemisorbed 4-nitrobenzenethiol (NBT),[15−18] accelerate enzyme catalysis,[19] and can trigger reactions with medical applications.[20−22] While detailed mechanisms for the catalysis of these reactions remain unclear, there is evidence that vibrational energy flow plays a central role in the kinetics of many of them. The NO stretch of NBT has been the subject of particular interest, as selective excitation of this mode has been recently observed to drive dissociation, where the extent to which the reaction can be accelerated by selective excitation depends on vibrational energy flow.[16] Picosecond time-resolved surface-enhanced Raman spectroscopy (SERS) carried out on NBT and other substituted benzenethiols attached to metal nanoparticles has provided information about vibrational dynamics and energy flow in these molecules.[23,24] Still, intriguing trends in the lifetimes of some of the vibrations that have been measured for different substituted benzenethiols remain unexplained, as do the relative contributions of intra- and intermolecular energy flow to the observed energy dynamics. In this letter, we report the results of quantum mechanical calculations of vibrational energy flow in NBT and four additional substituted benzenethiols attached to metal nanoparticles. We examine and clarify the contributions of intra- and intermolecular energy flow and their mechanisms, compare the computational results to recent experiments[23,24] that have monitored population dynamics, and discuss implications for the selective reactivity of NBT.

There has been much debate about mechanisms by which chemical reactions can be catalyzed by plasmonic nanoparticles, often focusing on the roles of hot charge carriers transferred to nearby molecules and photothermal effects.[25−33] Excitation sources include the plasmonic electric field, hot carriers, and local heating, and the nature and shape of the nanomaterials can impact reaction progress.[14] Regardless of how energy is introduced to the molecule attached to the plasmonic nanoparticle, vibrational dynamics and relaxation mediate chemical reaction kinetics.[34−43] The connection between vibrational relaxation and dissociation of NBT following plasmonic excitation has been made strikingly clear in a recent study by Kim and co-workers,[16] who have demonstrated selective excitation of the NO stretch of NBT attached to gold. The excess population depends sensitively on

Received: March 21, 2024
Revised: April 30, 2024
Accepted: May 9, 2024

the lifetime of this vibration. It is therefore important to examine the origin of the lifetime and what properties of NBT and other substituted benzenethiols control it. Beyond the lifetimes of the vibrational modes, the population dynamics of the vibrations in response to photothermal heating of the attached nanoparticles and comparison with experiments can provide a strong indicator of their role, if any, in initiating the reaction.

We present calculations of lifetimes of vibrational modes of 5 substituted benzenethiols: NBT, 4-methylbenzenethiol (MBT), 4-chlorobenzenethiol (CBT), biphenyl-4-thiol (BPT), and benzenethiol (BT). The lifetimes are computed quantum mechanically via a Fermi's golden rule approach. Mode frequencies and anharmonic constants used in the calculations are computed with MP2 for each molecule. While we compute the lifetimes of all vibrational modes of NBT, we focus on the three Raman-active modes of NBT studied experimentally by the Frontiera group.[23,24] For the other substituted benzenethiols, we again focus on the Raman-active modes studied experimentally. We find that the computed lifetimes of the 5 substituted benzenethiols are reasonably close to measured values and that the lifetime is largely mediated by intramolecular vibrational relaxation (IVR), not by energy transfer to other molecules, the rate of which we also determine computationally. Differences in lifetimes are found to arise from shifts in mode frequencies for different substituents attached to the benzenethiol.

Population dynamics of several modes of NBT in response to the excitation of plasmonic resonances of gold nanoparticles have been measured on the ps time scale.[23,24] To examine the population dynamics of NBT following photothermal heating of an attached metal nanoparticle, we adopt a master equation simulation approach, where rates of energy transfer between different vibrational states are computed using Fermi's golden rule, while rates of energy transfer between the molecule and surroundings are estimated using the results of nonequilibrium molecular dynamics (MD) simulations. Those simulations have been carried out in two parts. For NBT attached to gold (Figure 1), we simulate the temperature profile following rapid heating of gold to determine the rate of thermal transfer between the gold and NBT and snapshots of the temperature profile of any surrounding solvent molecules at different times during the simulation. For those temperatures, we then, in the second part, determine the time of vibrational energy transfer from a hot NBT molecule into the solvent, which in our simulations is either toluene, ethanol, or water.

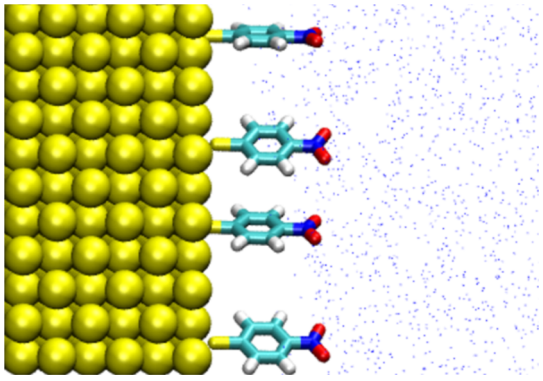

Figure 1. Illustration of NBT attached to a gold substrate, which can be gold nanoparticle or surface. In the MD simulations, NBT molecules are attached to gold surfaces in the presence of solvent, as depicted in this illustration as blue dots.

From the results of the MD simulations, we obtain time constants for energy transfer between the hot metal and NBT as well as time constants for energy transfer between NBT and surrounding molecules. These time constants are introduced into the master equation to model the population of vibrational modes of NBT attached to hot metal nanoparticles in contact with other molecules. We shall see that even with considerable heating of the attached metal, the population dynamics of NBT appear consistent with those found in the SERS[23,24] experiments only at very short times, within about 5 ps, after which the results are very different. We therefore conclude that the molecules are initially excited electronically, possibly by transfer of hot charge carriers.

In the following section, we provide information about the computational methods used in this study. In Section 3 we present and discuss the results. Concluding remarks appear in Section 4.

2. COMPUTATIONAL METHODS

2.1. Mode Lifetimes. The initial geometries of NBT, MBT, CBT, BPT, and BT were optimized using MP2/6-31G(d), followed by MP2/6-31G(d,p), and finally optimized with MP2/6-31G(2df,2p). The vibrational mode frequencies, anharmonic constants, and Raman spectra of all five molecules were calculated with MP2/6-31G(2df,2p) for the final geometries. All calculations were performed using the Gaussian 16 software package.[44] The superfine integration grid and a two-electron integration calculation accuracy of 10^{-13} were applied in all calculations.

The rate of relaxation of excess vibrational quanta in a mode, α, is determined in terms of mode frequencies, the anharmonic interactions with other modes of the molecule, computed with the MP2 calculations, and interactions with the environment of the molecule, obtained by MD simulations (below). The relaxation rate (W) arising from intramolecular interactions was estimated in terms of third-order anharmonic interactions using Fermi's golden rule calculation. In this approximation, the rate is the sum of two contributions, i.e., $W = W_d + W_c$[45−48]

$$W_d(\omega_\alpha) = \frac{\hbar}{16\omega_\alpha} \sum_{\beta,\gamma} \left\{ \frac{|\phi_{\alpha\beta\gamma}|^2 (1 + n_\beta + n_\gamma)(\Gamma_\alpha + \Gamma_\beta + \Gamma_\gamma)}{\omega_\beta \omega_\gamma \left[(\omega_\beta + \omega_\gamma - \omega_\alpha)^2 + \frac{1}{4}(\Gamma_\alpha + \Gamma_\beta + \Gamma_\gamma)^2 \right]} \right\} \tag{1a}$$

$$W_c(\omega_\alpha) = \frac{\hbar}{8\omega_\alpha} \sum_{\beta,\gamma} \left\{ \frac{|\phi_{\alpha\beta\gamma}|^2 (n_\beta - n_\gamma)(\Gamma_\alpha + \Gamma_\beta + \Gamma_\gamma)}{\omega_\beta \omega_\gamma \left[(\omega_\gamma - \omega_\beta - \omega_\alpha)^2 + \frac{1}{4}(\Gamma_\alpha + \Gamma_\beta + \Gamma_\gamma)^2 \right]} \right\} \tag{1b}$$

where subscripts d and c refer to decay and collision, respectively. W_d accounts for the rate of loss, or decay, of a vibrational quantum from mode α with the addition of quanta to modes β and γ. W_c accounts for the rate of loss of vibrational quanta from modes α and β with the addition of a quantum to mode γ. The analogous process in a solid involves

https://doi.org/10.1021/acs.jpcc.4c01873
J. Phys. Chem. C XXXX, XXX, XXX−XXX

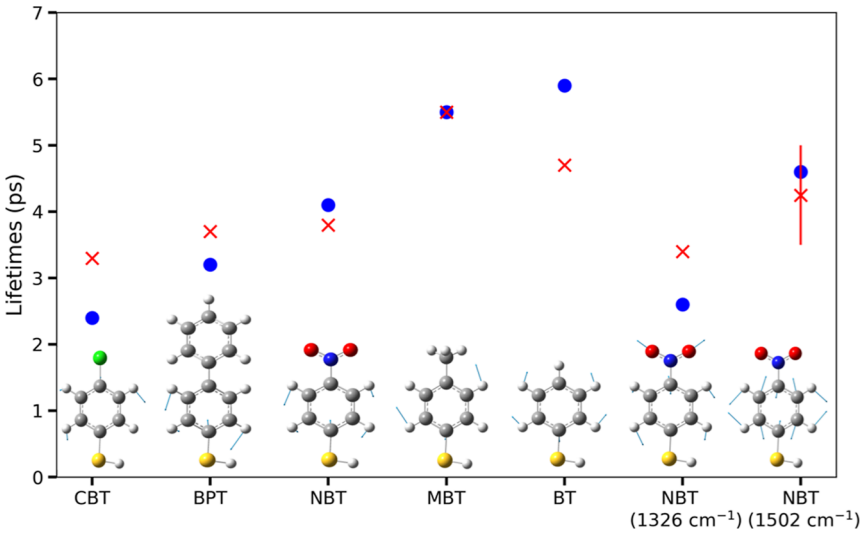

Figure 2. IVR lifetimes of the ≈1060 cm^{-1} mode computed (circles) for 5-substituted benzenethiols, shown with the modes themselves, and comparison (×) with experimental values from ref 24. For this mode, the molecules are listed from the shortest to the longest computed lifetime (left to right). Trend is nearly the same for the measured results. NO stretch of NBT at 1326 cm^{-1} and another mode at 1502 cm^{-1} is shown to the right with experimental values from ref 23.

the collision of phonons of modes α and β to generate a phonon in mode γ.[49] $\Phi_{\alpha\beta\gamma}$ are cubic anharmonic constants for coupling between modes $\alpha\beta\gamma$. The values of the cubic anharmonic constants are obtained from the ab initio calculations, as discussed above. Γ_β is the damping rate of mode β due to coupling to other modes and to the environment, n_α is the population of mode α, taken to be $n_\alpha = \left[\exp\left(\frac{\hbar\omega_\alpha}{k_B T}\right) - 1\right]^{-1}$. We use Γ_β = 6 cm^{-1} for each mode, corresponding to a damping rate of ≈1 ps^{-1}. The damping rate is due mainly to coupling to the metal, which we find in the MD simulations to give rise to a 1.3 ps lifetime, as discussed below. Other contributions include the ≈0.2 ps^{-1} rate of intramolecular energy transfer and ≈0.12 ps^{-1} rate of intermolecular energy transfer, the latter also found in the MD simulations. We note that we found in earlier work on solvated cyanophenylalanine that the results of eq 1a do not change significantly using a range of values from 0.2 to 1.5 ps^{-1}.[47] For relaxation from higher frequency modes, eq 1a contributes much more to the rate than eq 1b. We also plot the vibrational densities of states coupled by cubic anharmonic interactions in Figure S1.

A criterion for estimating the vibrational lifetime with Fermi's golden rule is that the product of the average coupling via anharmonic coupling and the density of states coupled by such modes be of order 1.[34] We have therefore checked that this criterion has been met for the molecules studied here at the energies we consider. Resonant coupling can be characterized by the relative magnitude of the cubic anharmonic constant to the frequency mismatch of the coupled modes ($\Delta\omega$), defined as $|\omega_\gamma + \omega_\beta - \omega_\alpha|$. The ratio of the magnitude of the anharmonic coupling to $\Delta\omega$ is the third-order Fermi resonance (TFR) parameter defined as[47,48]

$$\mathrm{TFR}_{\alpha\beta\gamma} = \left|\frac{\Phi_{\alpha\beta\gamma}}{\Delta\omega}\right| \tag{2}$$

We drop the subscripts for the TFR parameter and discuss the modes that are coupled in what follows. Modes are resonant when the TFR parameter is of order 1 or larger.

2.2. Master Equation Simulations of Population Dynamics. We model the population dynamics using a master equation approach to examine vibrational dynamics prior to the onset of steady-state thermal transport. Steady-state thermal transport in molecular interfaces and junctions has been extensively studied,[50−64] as has the onset of steady-state transport for some specific systems.[65−76] We calculate the population change with time arising from cubic anharmonic interactions within the molecule and linear coupling between the molecule and the nanoparticle and solvent. With cubic coupling, there are 4 terms that contribute to population change: (1) one quantum of mode α is converted to 2 quanta, one in mode β, and the rest in mode γ (where β and γ may be the same mode, so a 2:1 resonance); (2) one quantum of mode α combines with a quantum in mode β to add a quantum to γ; (3) one quantum is added to mode α from mode β and mode γ (where β and γ may be the same mode); and (4) one quantum is added to mode α and mode β from mode γ. The rate of process (j) is $\Gamma^{(j)}$, given by golden rule formulas (see Supporting Information) combining to give

$$\begin{aligned}\frac{dn_\alpha(t)}{dt} = &\sum_{\beta,\gamma}\left(\Gamma^{(3)}_{\alpha,\beta\gamma} + \Gamma^{(4)}_{\alpha,\beta\gamma} - \Gamma^{(1)}_{\alpha,\beta\gamma} - \Gamma^{(2)}_{\alpha,\beta\gamma}\right)\\ &- \sum_{\alpha,\omega_\alpha\le\omega_D} w_m\left(n_\alpha(t) - \langle n_\alpha\rangle_m\right)\\ &- \sum_{\alpha} w_s\left(n_\alpha(t) - \langle n_\alpha\rangle_s\right)\end{aligned} \tag{3}$$

The rate constants w_m and w_s correspond to population transfer between the metal and molecule and the molecule and surroundings, respectively. Their values have been set as for eq 1a, using the results of the MD simulations (below). The equilibrium population at the temperature of the metal (surroundings) is $\langle n_\alpha\rangle_m$ ($\langle n_\alpha\rangle_s$), and the Debye frequency (or a cutoff frequency) of the metal is ω_D, roughly 120 cm^{-1} for gold. We use a slightly higher value of 150 cm^{-1} to allow for

https://doi.org/10.1021/acs.jpcc.4c01873
J. Phys. Chem. C XXXX, XXX, XXX−XXX

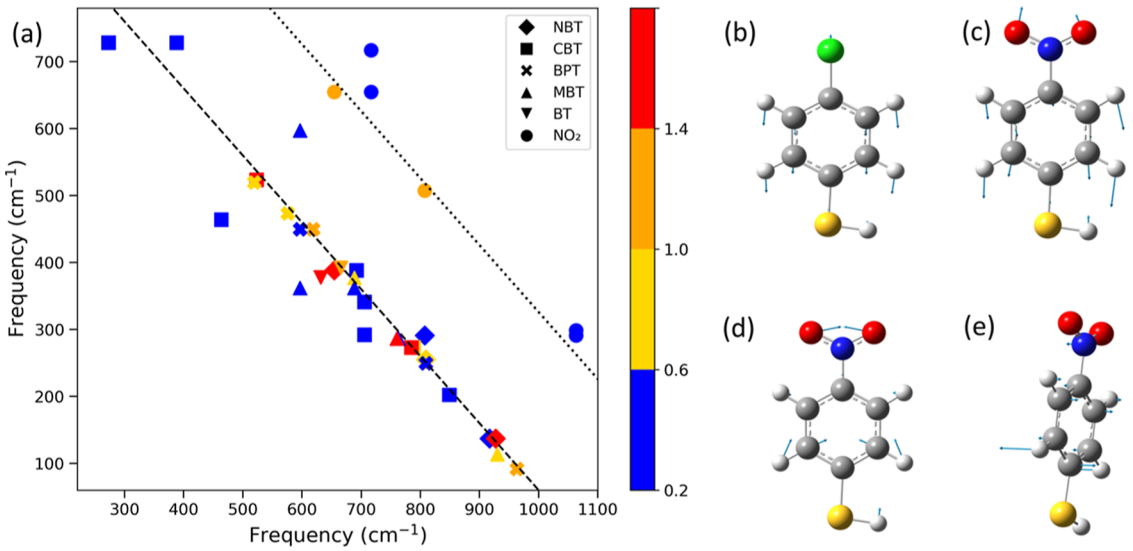

Figure 3. (a) TFR parameter values for some of the modes that mediate lifetimes of the roughly 1060 cm^{-1} mode. All parameter values at least 0.2 are indicated. However, significant contributions to IVR typically involve larger values, ≈1 or larger. The dashed line indicates the sum of the two frequencies plotted on the axes being 1060 cm^{-1} and the dotted line 1326 cm^{-1}, which correspond to the ring-breathing modes and NO stretch, respectively. Largest TFR parameters lie along these lines, as these are closest to resonance. Displacements of atoms of some of the modes involved in sizable TFR parameters are plotted in (b) 524 cm^{-1} mode of CBT, which mediates energy relaxation from the 1043 cm^{-1} mode via a 2:1 Fermi resonance; (c) 507 cm^{-1} mode combines with (d) 808 cm^{-1} mode to mediate the lifetime of the NO stretch of 1326 cm^{-1}; and (e) 655 cm^{-1} mode also contributes to lifetime of NO stretch via 2:1 Fermi resonance.

coupling to additional modes of the molecule, allowing for a broader phonon spectrum for the nanoparticles as compared to bulk systems; somewhat broader spectra have been used in other studies.[60] The rate constants $\Gamma^{(j)}$ depend on cubic anharmonic constants that are computed with MP2 (above). The initial population of each mode corresponds to the equilibrium population at 300 K.

3. RESULTS AND DISCUSSION

3.1. Mode Lifetimes. We have computed the lifetimes of the vibrational modes of NBT, CBT, BT, BPT, and MBT using eq 1a. The results are plotted in Figure 2, where we focus on the modes for which the lifetimes have been measured experimentally.[23,24] The lifetimes of other modes of NBT, which are used in the master equation simulations discussed below, are listed in the Supporting Information. In addition to lifetimes, we also show in Figure 2 images of the displacements of atoms for the vibrational modes that are listed.

Consider first the lifetimes computed for modes near 1060 cm^{-1}. The computed frequencies for this ring-breathing mode vary from 1053 cm^{-1} (BPT) to 1071 cm^{-1} (BT), somewhat lower than the experimental values near 1080 cm^{-1}. Despite this modest shift compared to experiments, we find the computed lifetimes to be reasonably close to those found experimentally. For CBT, BPT, NBT, MBT, and BT, we obtain lifetimes of 2.4, 3.2, 4.1, 5.5, and 5.9 ps, respectively. This can be compared with experimentally measured values of 3.3, 3.7, 3.8, 5.5, and 4.7 ps, respectively.[24] In addition to lifetimes that agree quite well with the experimental measurements, the trend that is seen, where the lifetime of CBT (2.4 ps) is the shortest and for BT (5.9 ps) and MBT (5.5 ps) is the longest, is nearly the same as that found in the experiments. We focus on this trend and its origins in what follows.

The golden rule calculation (eq 1a) explicitly accounts for coupling among intramolecular degrees of freedom, and the lifetimes are largely due to IVR. We note that eq 1a contributes much more to the rate of IVR of the ring-breathing modes than eq 1b, with the latter contributing on average 8% to the rate. The origin of the differences among the 5 lifetimes is due to frequency shifts of a relatively small number of modes, which when combined form a resonance with the ≈1060 cm^{-1} mode due to third-order anharmonic coupling. Resonant coupling via third-order anharmonic interactions appears to be stronger for CBT than the others. We analyze modes that primarily mediate the lifetime of the ≈1060 cm^{-1} mode of each molecule, then return to the other modes of NBT that appear in Figure 2.

We plot in Figure 3, the TFR parameter for modes coupled to the ≈1060 cm^{-1} ring-breathing mode of each molecule we study, as well as the NO stretch of NBT, where values of 0.2 or greater are indicated. The parameter values are also listed in Table S3. Consider first coupling to the ≈1060 cm^{-1} mode. For CBT, the largest TFR is for the 2:1 resonance with the 523 cm^{-1} mode. For BPT, the largest values include coupling with various pairs of modes, including 450 and 619, 473 and 576, 92 and 964 cm^{-1}, and a 2:1 Fermi resonance with the 519 cm^{-1} mode. For NBT, the largest TFR values are for 137 and 927, 388 and 655, and 255 and 809 cm^{-1}. For MBT, the largest value corresponds to 286 and 760 cm^{-1}. For BT, it is large for 378 and 632 cm^{-1} and for 392 and 666 cm^{-1}. For modes coupled to the NO stretch of NBT (1326 cm^{-1}) the largest TFR, also plotted in Figure 3, is for 507 and 808 cm^{-1}, and a somewhat smaller TFR for the 2:1 Fermi resonance of with the 655 cm^{-1} mode. We note that a small shift in the frequency of the 655 cm^{-1} mode, which can change slightly with a different basis set size, has a significant effect on the TFR parameter. Using the smaller MP2/6-31g(2df,p) basis set, the mode frequency shifts to 651 cm^{-1} and even with only a small change in the anharmonic coupling constant (≈10%), the TFR parameter increases by a factor of ≈6 due to the small frequency change. Overall, we see that a relatively small number of modes pair to form a resonance with either the

https://doi.org/10.1021/acs.jpcc.4c01873
J. Phys. Chem. C XXXX, XXX, XXX−XXX

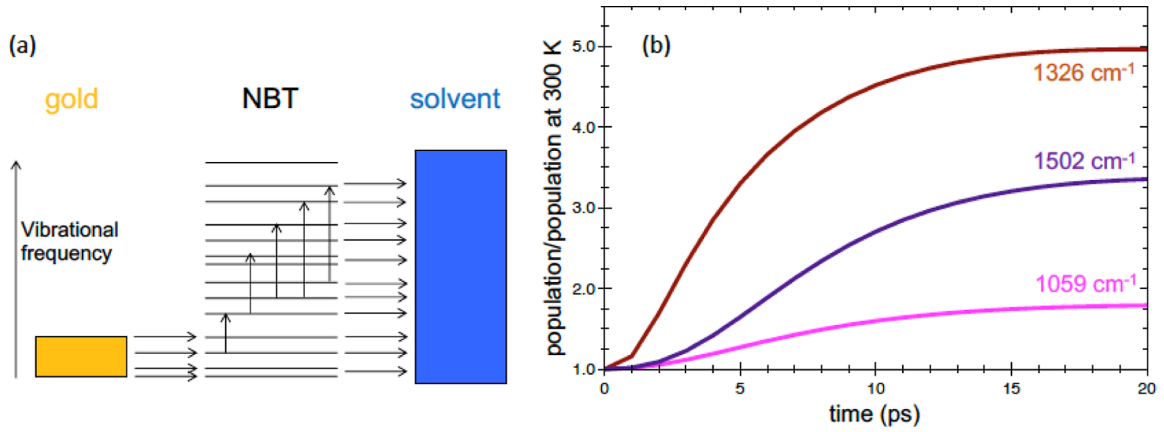

Figure 4. (a) Schematic energy diagram illustrating relative energies, including phonon band of gold, with cutoff frequency of 150 cm^{-1}, vibrational modes of NBT, where the Raman-active modes probed experimentally lie above 1000 cm^{-1}, and the environment, indicated as solvent. The arrows indicate the flow of heat at early times in the master equation simulations, as phonons are transferred from the hot metal to the molecules, in which up-conversion occurs by anharmonic interactions, as energy transfers to the environment. (b) Master equation simulation results for population dynamics of 3 Raman-active modes of NBT, indicated in the figure where the nanoparticles to which the molecules are attached are initially heated (see text). The population of the mode relative to the population at 300 K is plotted to 20 ps, by which time it appears that steady state is reached for the conditions of the simulations.

≈1060 cm^{-1} of these molecules or the NO stretch of NBT, and that the largest TFR values lie where the modes are nearly resonant. These modes largely mediate rates of energy transfer, as we now discuss.

The nature of some of the modes that give rise to large TFR parameter values is also shown in Figure 3. The 523 cm^{-1} mode of CBT is depicted, which is close to half the frequency of the 1049 cm^{-1} mode, as shown in Figure 2. The relatively short lifetime of the 1049 cm^{-1} mode of CBT, compared to the ring-breathing mode of the other molecules, is due to the 2:1 Fermi resonance with the 523 cm^{-1} mode, which accounts for about 70% of its lifetime. Another resonance, due to the cubic anharmonic coupling of the 1049 cm^{-1} mode with the 273 and 785 cm^{-1} modes of CBT, accounts for most of the rest of the lifetime.

The lifetime of the 1053 cm^{-1} mode of BPT, 3.2 ps, is somewhat longer than the 2.4 ps lifetime of the 1049 cm^{-1} mode of CBT. A mode very similar to the one most responsible for the lifetime in CBT shifts to 519 cm^{-1} in BPT, so that the 2:1 resonance between the 1053 cm^{-1} mode of BPT and the 519 cm^{-1} mode of BPT is more detuned than the corresponding modes of CBT. In addition to this 2:1 resonance, anharmonic coupling between the 1053 cm^{-1} mode and the 450 and 619 cm^{-1} modes of BPT also contributes to the lifetime of the 1053 cm^{-1} mode.

The corresponding ring-breathing mode ≈1060 cm^{-1} of the other molecules relaxes significantly more slowly in MBT and BT, where the mode frequencies are 1054 and 1071 cm^{-1}, respectively. There is no mode that appears like the 524 cm^{-1} mode of CBT in those molecules anywhere near 500 cm^{-1}. Instead, one finds the frequency of a similar mode of MBT to be 599 cm^{-1} and of BT to be 389 cm^{-1}. There is therefore no 2:1 resonance with these modes that can contribute to the lifetime of the 1054 and 1071 cm^{-1} modes. For MBT, the lifetime is mediated by anharmonic coupling to a pair of modes with frequencies 286 and 760 cm^{-1}, as well as a second pair, 377 and 689 cm^{-1}. For BT, the lifetime is mediated by the anharmonic coupling to a pair of modes with frequencies 392 and 665 cm^{-1}. The combinations of modes that most influence the lifetimes of the ring-breathing modes are listed in the Supporting Information (Table S4).

We now consider the higher frequency modes of NBT, as shown in Figure 2. We compute the lifetime of the NO stretch (1326 cm^{-1}) with eq 1a to be 2.6 ps, which is reasonably close to the measured value of 3.4 ps. We find two major pathways for energy flow from this mode that mediate its lifetime. One is a 2:1 Fermi resonance with a 655 cm^{-1} mode, which is shown in Figure 3. A second is via anharmonic coupling with the 507 and 808 cm^{-1} modes of NBT, also shown in Figure 3. All these modes involve significant displacement of NO_2.

We note that the NO stretch can be selectively excited by plasmonic excitation of the attached metal, which can be exploited to facilitate a NBT decomposition reaction.[16] The extent to which the population of the NO stretch can be enhanced and the reaction accelerated depends sensitively on the lifetime of this mode. The population of the mode, n_{NO}, exceeds the equilibrium population, $\langle n_{NO}\rangle$ by the ratio of the rate of excitation, w_{ex}, to the rate, w_{rel}, of relaxation rate due to IVR, $n_{NO} - \langle n_{NO}\rangle = w_{ex}/w_{rel}$.[16] It would thus be of interest to explore ways to enhance the lifetime, perhaps by introducing chemical groups that might shift the frequency of the 655 cm^{-1} mode out of 2:1 resonance with the NO stretch, a possibility we are presently investigating.

The highest frequency Raman-active mode of NBT that has been measured[23] is computed to have a frequency of 1502 cm^{-1}. For this mode, we calculate a lifetime of 4.6 ps, which lies within the range of 3−5 ps found experimentally.[23] We find the lifetime to be determined mainly by anharmonic coupling to a relatively low and relatively high frequency mode, specifically the 179 and 1311 cm^{-1} modes, which, when combined are nearly resonant with the 1502 cm^{-1} mode.

Just as small shifts in frequency obtained using basis sets of different sizes can affect the value of the TFR parameter in some cases, discussed above, they can also affect the value of the lifetime. Using the smaller MP2/6-31g(2df,p) basis set, we find the lifetime to change within 0.8 ps for all modes discussed above, except for the ring-breathing mode of MBT, for which the lifetime is longer by 1.6 ps using the smaller basis set. The relative order of the lifetimes of the ring-breathing mode for

https://doi.org/10.1021/acs.jpcc.4c01873
J. Phys. Chem. C XXXX, XXX, XXX−XXX

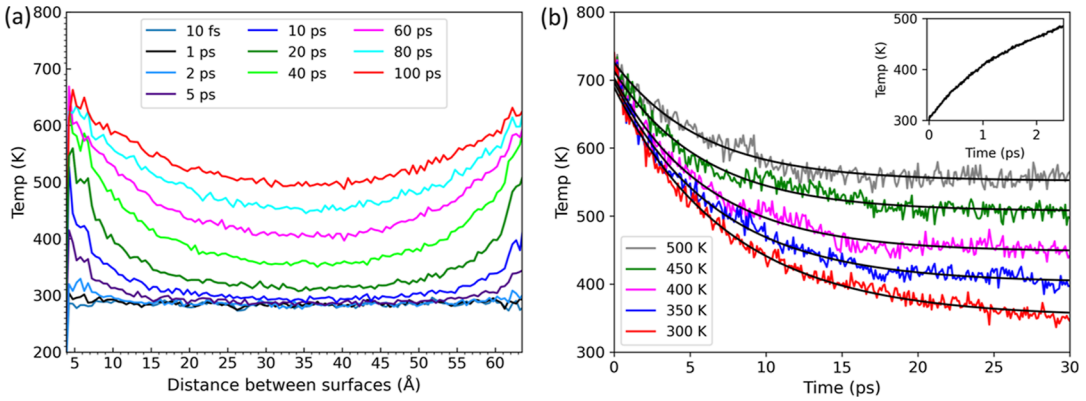

Figure 5. (a) Time-dependent heating of solvent (toluene) due to thermal excitation. (b) Results of thermal cooling simulations of NBT in toluene; inset shows heating of NBT molecules in response to heating of gold.

the 5 benzenethiols follows the same trend as the experiments and the same trend we found with the larger basis set. The change in the NO stretch lifetime is shorter by 1.2 ps using the smaller basis set. The mode lifetimes obtained using the two basis sets for which results have been compared are listed in Table S5.

3.2. Vibrational Population Dynamics. Having examined the lifetimes of vibrational modes of these molecules, we turn to the population dynamics of modes of NBT in response to photothermal heating of the attached nanoparticles and comparison with experiments to examine their role, if any, in initiating reactions. We have simulated the population dynamics of 3 Raman-active modes of NBT probed experimentally, which in the calculations are 1052, 1326, and 1502 cm^{-1}. For the simulations that we carried out, the system is assumed to have equilibrated to 300 K and photoexcitation, at time t = 0, heats the gold nanoparticles to which NBT molecules are attached. We find at early times that the population dynamics mimic to some extent those observed in the experiments of Frontiera and co-workers[23,24] if, in the simulations, the gold nanoparticles are initially heated by several hundred kelvin. We illustrate this by heating them to 700 K initially, while the rest of the system, i.e., solvent molecules in contact with NBT, is taken initially at 300 K. Though over time, the nanoparticles will cool, even a single nanoparticle comparable in size to those studied experimentally requires more than 10 ns to cool,[77] and clusters of them cool over much longer times. These times are much longer than the simulation times reported here. Population dynamics we obtain from the master equation simulations to 20 ps are shown in Figure 4.

Under the conditions applied in the simulations, we find the population of the three modes to rise rapidly, in 5−10 ps, then plateau as the steady state is reached. At very short times, only low-frequency modes of the molecule are populated due to the low Debye frequency of gold. Higher frequency modes become populated via up-conversion due mainly to the anharmonic interactions. The rise time that we observe in the population of these modes is commensurate with what is observed experimentally, also when allowing for limits in the experimental resolution of a few ps. For example, the relative population of the ≈1080 cm^{-1} mode is seen to rise by roughly 40−50% over the first few ps,[24] comparable to the increase we observe for the 1052 cm^{-1} mode in the first few ps. For the other modes, for which the rise was reported as an effective temperature in ref 23, the increase is commensurate with the population increase we find in the first few ps.

However, in the experiments, the population of these modes is observed to decrease sharply over the next 10 ps,[23,24] in contrast to the plateau seen in Figure 4, which reflects a new steady-state population in the simulations. In fact, as we discuss below and show in Figure 5, the surroundings can heat up significantly over 20 ps, so that the population of the modes plotted in Figure 4 would be expected to rise further. Due to the difference in the simulated result, which accounts for (substantial) photothermal heating, the experimental observation that the population decays at a rate that we have shown above is consistent with IVR indicates that the modes are not initially populated by photothermal heating.

We have also simulated the cooling rate of NBT due to coupling to a molecular environment, which could correspond to the solvent or other NBT molecules. The decay of energy in NBT, heated to 700 K due to coupling to the hot gold, into other molecules at different temperatures is plotted in Figure 5b. The decay of energy in Figure 5b, when fit to an exponential, provides the rate constant for energy transfer to the molecular environment from NBT at different environmental temperatures. Near 300 K, the decay time is 8 ps and changes somewhat as the temperature rises (Table S2). The time for energy transfer from the hot metal to NBT, about 1.3 ps, is also shown in Figure 5b. The 1.3 ps time constant for heating NBT by the gold and the 8 ps time constant for energy transfer to the solvent are used in the master equation simulations. There are modest differences in the cooling rate with temperature (Table S2), and the temperature of the molecules surrounding the gold nanoparticles changes on the picosecond time scale in the simulations, as seen in Figure 5a. However, the cooling rate would need to increase rapidly for the mode populations plotted in Figure 4b to decrease with time, as seen in the experiments, and such a rapid increase in the cooling rate is not found in the results of the cooling simulations.

4. CONCLUSIONS

In summary, plasmon-assisted catalysis has been found experimentally to depend on the lifetimes of vibrational modes that are selectively excited and can facilitate reactions.[16] We have calculated rates of vibrational energy flow in 5 substituted benzenethiols attached to plasmonic nanoparticles to identify molecular properties that influence the lifetime, such as functional groups and their effect on resonances, as

https://doi.org/10.1021/acs.jpcc.4c01873
J. Phys. Chem. C XXXX, XXX, XXX−XXX

well as the relative contributions of intra- and intermolecular energy flow. For the calculation of rates of vibrational relaxation, we have accounted for anharmonic coupling among the vibrational modes of the substituted benzenethiol and linear coupling to the attached metal nanoparticle and other molecules in the environment. The lifetimes are largely due to IVR and agree well with experimental values. Trends in the lifetimes for the substituted benzenethiols observed in experiments[24] are reproduced and explained by shifts in resonances involving a few vibrational modes due to the different substituents.

We have also investigated the extent to which photothermal effects trigger reactions by simulating what the population dynamics of NBT would look like if the molecules were heated by plasmonic nanoparticles. The results bear some resemblance to experimental measurements[23,24] at very early times but are inconsistent with experiments after about 5−10 ps. We therefore conclude that the molecules are excited electronically, as suggested previously,[23] probably via the transfer of hot charge carriers from the metal nanoparticle to the molecule.

Finally, we have identified the modes of NBT that mediate the lifetime of the NO stretch, the value of which is in good agreement with the experiment. That lifetime mediates the extent to which the chemistry of NBT can be controlled via selective excitation of the NO stretch.[16] It is of interest in future work to identify factors that can shift the frequency of modes into which energy flows from the NO stretch, such as electric fields or substituents,[48,78] and can potentially enhance the lifetime of this mode and facilitate reaction. The ability to shift pathways of vibrational energy flow may also help facilitate other reactions in much larger molecules, such as proteins.[19,79]

■ ASSOCIATED CONTENT

Supporting Information

The Supporting Information is available free of charge at https://pubs.acs.org/doi/10.1021/acs.jpcc.4c01873.

Details of master equation and MD simulations; lists of mode frequencies of NBT, CBT, MBT, BPT, and BT; lifetimes of modes of NBT; TFR parameter values; modes that mediate lifetimes of ring-breathing modes; densities of mode combinations and overtones; and force field parameters (PDF)

■ AUTHOR INFORMATION

Corresponding Author

David M. Leitner − *Department of Chemistry, University of Nevada, Reno, Nevada 89557, United States;* orcid.org/0000-0002-3105-818X; Email: dml@unr.edu

Authors

Humanath Poudel − *Department of Chemistry, University of Nevada, Reno, Nevada 89557, United States*

Pathick Halder Shaon − *Department of Chemistry, University of Nevada, Reno, Nevada 89557, United States*

Complete contact information is available at: https://pubs.acs.org/10.1021/acs.jpcc.4c01873

Notes

The authors declare no competing financial interest.

■ ACKNOWLEDGMENTS

Support from NSF grant CHE-2245240 is gratefully acknowledged. The authors are grateful to the Cyberinfrastructure Team in the Office of Information Technology at UNR for access to the Pronghorn HPC cluster, with allocation supported by UNR Student Technology Fees.

■ REFERENCES

(1) Warkentin, C. L.; Yu, Z.; Sarkar, A.; Frontiera, R. R. Decoding Chemical and Physical Processes Driving Plasmonic Photocatalysis Using Surface-Enhanced Raman Spectroscopies. *Acc. Chem. Res.* **2021**, *54*, 2457−2466.

(2) Boerigter, C.; Aslam, U.; Linic, S. Mechanism of Charge Transfer from Plasmonic Nanostructures to Chemically Attached Materials. *ACS Nano* **2016**, *10*, 6108−6115.

(3) Kazuma, E.; Kim, Y. Mechanistic Studies of Plasmon Chemistry on Metal Catalysts. *Angew. Chem., Int. Ed.* **2019**, *58*, 4800−4808.

(4) Zhang, Z.; Zhang, C.; Zheng, H.; Xu, H. Plasmon-Driven Catalysis on Molecules and Nanomaterials. *Acc. Chem. Res.* **2019**, *52*, 2506−2515.

(5) Hassan, S.; Schade, M.; Shaw, C. P.; Lévy, R.; Hamm, P. Response of Villin Headpiece-Capped Gold Nanoparticles to Ultrafast Laser Heating. *J. Phys. Chem. B* **2014**, *118*, 7954−7962.

(6) Kim, H.; Park, H.; Kang, M.; Park, J. Y. Plasmonic Hot Carrier-Driven Photoelectrochemical Water Splitting on Antenna-Reactor Pt/Ag/TiO2 Schottky Nanodiodes. *J. Chem. Phys.* **2022**, *157*, 084701.

(7) Jiang, W.; Low, B. Q. L.; Long, R.; Low, J.; Loh, H.; Tang, K. Y.; Chai, C. H. T.; Zhu, H.; Zhu, H.; Li, Z.; et al. Active Site Engineering on Plasmonic Nanostructures for Efficient Photocatalysis. *Nano Lett.* **2023**, *17*, 4193−4229.

(8) Jain, P. K.; Qian, W.; El-Sayed, M. A. Ultrafast Cooling of Photoexcited Electrons in Gold Nanoparticle-Thiolated DNA Conjugates Involves the Dissociation of the Gold-Thiol Bond. *J. Am. Chem. Soc.* **2006**, *128*, 2426−2433.

(9) Al-Zubeidi, A.; Ostovar, B.; Carlin, C. C.; Li, B. C.; Lee, S. A.; Chiang, W. Y.; Gross, N.; Dutta, S.; Misiura, A.; Searles, E. K.; et al. Mechanism for Plasmon-Generated Solvated Electrons. *Proc. Natl. Acad. Sci. U.S.A.* **2023**, *120*, No. e2217035120.

(10) Nan, L.; Giraldez-Martinez, J.; Stefancu, A.; Zhu, L.; Liu, M.; Govorov, A. O.; Besteiro, L. V.; Cortes, E. Investigating Plasmonic Catalysis Kinetics on Hot-Spot Engineered Nanoantennae. *Nano Lett.* **2023**, *23*, 2883−2889.

(11) Lee, J.; Mubeen, S.; Ji, X.; Stucky, G. D.; Moskovits, M. Plasmonic Photoanodes for Solar Water Splitting with Visible Light. *Nano Lett.* **2012**, *12*, 5014−5019.

(12) Zhang, Y.; He, S.; Guo, W.; Hu, Y.; Huang, J.; Mulcahy, J. R.; Wei, W. D. Surface-Plasmon-Driven Hot Electron Photochemistry. *Chem. Rev.* **2018**, *118*, 2927−2954.

(13) Brongersma, M. L.; Halas, N. J.; Nordlander, P. Plasmon-Induced Hot Carrier Science and Technology. *Nat. Nanotechnol.* **2015**, *10*, 25−34.

(14) Kazuma, E. Key Factors for Controlling Plasmon-Induced Chemical Reactions on Metal Surfaces. *J. Phys. Chem. Lett.* **2024**, *15*, 59−67.

(15) Sarhan, R. M.; Koopman, W.; Schuetz, R.; Schmid, T.; Liebig, F.; Koetz, J.; Bargheer, M. The Importance of Plasmonic Heating for the Plasmon-Driven Photodimerization of 4-Nitrothiophenol. *Sci. Rep.* **2019**, *9*, 3060.

(16) Shin, H.-H.; Jeong, J.; Nam, Y.; Lee, K. S.; Yeon, G. J.; Lee, H.; Lee, S. Y.; Park, S.; Park, H.; Lee, J. Y.; Kim, Z. H. Vibrationally Hot Reactants in a Plasmon-Assisted Chemical Reaction. *J. Am. Chem. Soc.* **2023**, *145*, 12264−12274.

(17) Schürmann, R.; Luxford, T. F. M.; Vinklárek, I. S.; Kočišek, J.; Zawadzki, M.; Bald, I. Interaction of 4-Nitrothiophenol with Low Energy Electrons: Implications for Plasmon Mediated Reactions. *J. Chem. Phys.* **2020**, *153*, 104303.

(18) Qiu, L.; Pang, G. A.; Zheng, G.; Bauer, D.; Wieland, K.; Haisch, C. Kinetic and Mechanistic Investigation of the Photocatalyzed

Surface Reduction of 4-Nitrothiophenol Observed on a Silver Plasmonic Film Via Surface-Enhanced Raman Scattering. *ACS Appl. Mater. Interfaces* **2020**, *12*, 21133−21142.
(19) Kozlowski, R.; Zhao, J.; Dyer, R. B. Acceleration of Catalysis in Dihydrofolate Reductase by Transient, Site-Specific Photothermal Excitation. *Proc. Natl. Acad. Sci. U.S.A.* **2021**, *118*, No. e2014592118.
(20) Qin, Z.; Bischof, J. C. Thermophysical and Biological Responses of Gold Nanoparticle Laser Heating. *Chem. Soc. Rev.* **2012**, *41*, 1191−1217.
(21) Luo, B.; Wang, W.; Zhao, Y.; Zhao, Y. Hot-Electron Dynamics Mediated Medical Diagnosis and Therapy. *Chem. Rev.* **2023**, *123*, 10808−10833.
(22) Dreaden, E. C.; Austin, L. A.; Mackey, M. A.; El-Sayed, M. A. Size Matters: Gold Nanoparticles in Targeted Cancer Drug Delivery. *Ther. Deliv.* **2012**, *3*, 457−478.
(23) Keller, E. L.; Frontiera, R. R. Ultrafast Nanoscale Raman Thermometry Proves Heating Is Not a Primary Mechanism for Plasmon-Driven Photocatalysis. *ACS Nano* **2018**, *12*, 5848−5855.
(24) Yu, Z.; Frontiera, R. R. Intermolecular Forces Dictate Vibrational Energy Transfer in Plasmonic-Molecule Systems. *ACS Nano* **2022**, *16*, 847−854.
(25) Golubev, A. A.; Khlebtsov, B. N.; Rodriguez, R. D.; Chen, Y.; Zahn, D. R. T. Plasmonic Heating Plays a Dominant Role in the Plasmon-Induced Photocatalytic Reduction of 4-Nitrobenzenethiol. *J. Phys. Chem. C* **2018**, *122*, 5657−5663.
(26) Zhou, L.; Swearer, D. F.; Zhang, C.; Robatjazi, H.; Zhao, H.; Henderson, L.; Dong, L.; Christopher, P.; Carter, E. A.; Nordlander, P.; et al. Quantifying Hot Carrier and Thermal Contributions in Plasmonic Photocatalysis. *Science* **2018**, *362*, 69−72.
(27) Zhou, L.; Lou, M.; Bao, J. L.; Zhang, C.; Liu, J. G.; Martirez, J. M. P.; Tian, S.; Yuan, L.; Swearer, D. F.; Robatjazi, H.; et al. Hot Carrier Multiplication in Plasmonic Photocatalysis. *Proc. Natl. Acad. Sci. U.S.A.* **2021**, *118*, No. e2022109118.
(28) Koopman, W.; Sarhan, R. M.; Stete, F.; Schmitt, C. N. Z.; Bargheer, M. Decoding the Kinetic Limitations of Plasmon Catalysis: The Case of 4-Nitrothiophenol Dimerization. *Nanoscale* **2020**, *12*, 24411−24418.
(29) Dubi, Y.; Un, I. W.; Sivan, Y. Thermal Effects - an Alternative Mechanism for Plasmon-Assisted Photocatalysis. *Chem. Sci.* **2020**, *11*, 5017−5027.
(30) Baffou, G.; Bordacchini, I.; Baldi, A.; Quidant, R. Simple Experimental Procedures to Distinguish Photothermal from Hot-Carrier Processes in Plasmonics. *Light: Sci. Appl.* **2020**, *9*, 108.
(31) Keshavamurthy, S. Eigenstates of Thiophosgene near the Dissociation Threshold: Deviations from Ergodicity. *J. Phys. Chem. A* **2013**, *117*, 8729−8736.
(32) Wu, Y.; Yang, M.; Ueltschi, T. W.; Mosquera, M. A.; Chen, Z.; Schatz, G. C.; VanDuyne, R. P. Sers Study of the Mechanism of Plasmon-Driven Hot Electron Transfer between Gold Nanoparticles and Pcbm. *J. Phys. Chem. C* **2019**, *123*, 29908−29915.
(33) Dubi, Y.; Un, I. W.; Baraban, J. H.; Sivan, Y. Distinguishing Thermal from Non-Thermal Contributions to Plasmonic Hydrodefluorination. *Nat. Catal.* **2022**, *5*, 244−246.
(34) Leitner, D. M. Quantum Ergodicity and Energy Flow in Molecules. *Adv. Phys.* **2015**, *64*, 445−517.
(35) Leitner, D. M. Heat Transport in Molecules and Reaction Kinetics: The Role of Quantum Energy Flow and Localization. *Adv. Chem. Phys.* **2005**, *130B*, 205−256.
(36) Leitner, D. M. Influence of Quantum Energy Flow and Localization on Molecular Isomerization in Gas and Condensed Phases. *Int. J. Quantum Chem.* **1999**, *75*, 523−531.
(37) Karmakar, S.; Keshavamurthy, S. Intramolecular Vibrational Energy Redistribution and the Quantum Ergodicity Transition: A Phase Space Perspective. *Phys. Chem. Chem. Phys.* **2020**, *22*, 11139−11173.
(38) Karmakar, S.; Yadav, P. K.; Keshavamurthy, S. Stable Chaos and Delayed Onset of Statisticality in Unimolecular Dissociation Reactions. *Commun. Chem.* **2020**, *3*, 4.
(39) Mondal, S.; Keshavamurthy, S. Phase Space Perspective on a Model for Isomerization in an Optical Cavity. *J. Chem. Phys.* **2023**, *159*, 074106.
(40) Berrios, E.; Pratt, S.; Tripathi, P.; Gruebele, M. More Protected Vibrational States at the Dissociation Limit of Sccl2. *J. Phys. Chem. A* **2013**, *117*, 12082−12090.
(41) Strickler, B.; Gruebele, M. Vibrational State Structure of Sccl2 from the Zero Point to the First Dissociation Limit. *Phys. Chem. Chem. Phys.* **2004**, *6*, 3786−3800.
(42) Zhang, C.; Wolynes, P.; Logan, D. E.; Wolynes, P. G. Surface Crossing and Energy Flow in Many-Dimensional Quantum Systems. *Proc. Natl. Acad. Sci. U.S.A.* **2023**, *120*, No. e2221690120.
(43) Leitner, D. M.; Wolynes, P. G. Quantum Energy Flow During Molecular Isomerization. *Chem. Phys. Lett.* **1997**, *280*, 411−418.
(44) Frisch, M. J.; Trucks, G. W.; Schlegel, H. B.; Scuseria, G. E.; Robb, M. A.; Cheeseman, J. R.; Scalmani, G.; Barone, V.; Petersson, G. A.; Nakatsuji, H.; et al. *Gaussian 16*, Revision 16; Gaussian, Inc.: Wallingford CT, 2016.
(45) Fabian, J.; Allen, P. B. Anharmonic Decay of Vibrational States in Amorphous Silicon. *Phys. Rev. Lett.* **1996**, *77*, 3839−3842.
(46) Yu, X.; Leitner, D. M. Vibrational Energy Transfer and Heat Conduction in a Protein. *J. Phys. Chem. B* **2003**, *107*, 1698−1707.
(47) Pandey, H. D.; Leitner, D. M. Vibrational States and Nitrile Lifetimes of Cyanophenylalanine Isotopomers in Solution. *J. Phys. Chem. A* **2018**, *122*, 6856−6863.
(48) Maitra, A.; Sarkar, S.; Leitner, D. M.; Dawlaty, J. M. Electric Fields Influence Intramolecular Vibrational Energy Relaxation and Line Widths. *J. Phys. Chem. Lett.* **2021**, *12*, 7818−7825.
(49) Maradudin, A. A.; Fein, A. E. Scattering of Neutrons by an Anharmonic Crystal. *Phys. Rev.* **1962**, *128*, 2589−2608.
(50) Leitner, D. M.; Pandey, H. D.; Reid, K. M. Energy Transport across Interfaces in Biomolecular Systems. *J. Phys. Chem. B* **2019**, *123*, 9507−9524.
(51) Pandey, H. D.; Leitner, D. M. Thermalization and Thermal Transport in Molecules. *J. Phys. Chem. Lett.* **2016**, *7*, 5062−5067.
(52) Pandey, H. D.; Leitner, D. M. Vibrational Energy Transport in Molecules and the Statistical Properties of Vibrational Modes. *Chem. Phys.* **2017**, *482*, 81−85.
(53) Pandey, H. D.; Leitner, D. M. Influence of Thermalization on Thermal Conduction through Molecular Junctions: Computational Study of Peg Oligomers. *J. Chem. Phys.* **2017**, *147*, 084701.
(54) Neidhart, S. M.; Gezelter, J. D. Thermal Transport Is Influenced by Nanoparticle Morphology: A Molecular Dynamics Study. *J. Phys. Chem. C* **2018**, *122*, 1430−1436.
(55) Shavalier, S. A.; Gezelter, J. D. Thermal Transport in Citrate-Capped Gold Interfaces Using a Polarizable Force Field. *J. Phys. Chem. C* **2022**, *126*, 12742−12754.
(56) Stocker, K. M.; Neidhart, S. M.; Gezelter, J. D. Interfacial Thermal Conductance of Thiolate-Protected Gold Nanospheres. *J. Appl. Phys.* **2016**, *119*, 025106.
(57) Foley, B. M.; Gorham, C. S.; Duda, J. C.; Cheaito, R.; Szwejkowski, C. J.; Constantin, C.; Kaehr, B.; Hopkins, P. E. Protein Thermal Conductivity Measured in the Solid State Reveals Anharmonic Interactions of Vibrations in a Fractal Structure. *J. Phys. Chem. Lett.* **2014**, *5*, 1077−1082.
(58) Segal, D.; Agarwalla, B. K. Vibrational Heat Transport in Molecular Junctions. *Annu. Rev. Phys. Chem.* **2016**, *67*, 185−209.
(59) Li, Q.; Strange, M.; Duchemin, I.; Donadio, D.; Solomon, G. C. A Strategy to Suppress Phonon Transport in Molecular Junctions Using Π-Stacked Systems. *J. Phys. Chem. C* **2017**, *121*, 7175−7182.
(60) Segal, D.; Nitzan, A.; Hänggi, P. Thermal Conductance through Molecular Wires. *J. Chem. Phys.* **2003**, *119*, 6840−6855.
(61) Wang, J. J.; Gong, J.; McGaughey, A. J. H.; Segal, D. Simulations of Heat Transport in Single-Molecule Junctions: Investigations of the Thermal Diode Effect. *J. Chem. Phys.* **2022**, *157*, 174105.
(62) Leitner, D. M. Energy Flow in Proteins. *Annu. Rev. Phys. Chem.* **2008**, *59*, 233−259.

https://doi.org/10.1021/acs.jpcc.4c01873
J. Phys. Chem. C XXXX, XXX, XXX−XXX

(63) Leitner, D. M. Thermal Boundary Conductance and Thermal Rectification in Molecules. *J. Phys. Chem. B* **2013**, *117*, 12820−12828.
(64) Reid, K. M.; Pandey, H. D.; Leitner, D. M. Elastic and Inelastic Contributions to Thermal Transport between Chemical Groups and Thermal Rectification in Molecules. *J. Phys. Chem. C* **2019**, *123*, 6256−6264.
(65) Wang, Z.; Carter, J. A.; Lagutchev, A.; Koh, Y. K.; Seong, N.-H.; Cahill, D. G.; Dlott, D. D. Ultrafast Flash Thermal Conductance of Molecular Chains. *Science* **2007**, *317*, 787−790.
(66) Leitner, D. M.; Pandey, H. D. Asymmetric Energy Flow in Liquid Alkylbenzenes: A Computational Study. *J. Chem. Phys.* **2015**, *143*, 144301.
(67) Pein, B. C.; Sun, Y.; Dlott, D. D. Unidirectional Vibrational Energy Flow in Nitrobenzene. *J. Phys. Chem. A* **2013**, *117*, 6066−6072.
(68) Pein, B. C.; Sun, Y.; Dlott, D. D. Controlling Vibrational Energy Flow in Liquid Alkylbenzenes. *J. Phys. Chem. B* **2013**, *117*, 10898−10904.
(69) Leitner, D. M.; Buchenberg, S.; Brettel, P.; Stock, G. Vibrational Energy Flow in the Villin Headpiece Subdomain: Master Equation Simulations. *J. Chem. Phys.* **2015**, *142*, 075101.
(70) Leong, T. X.; Qasim, L. N.; Mackin, R. T.; Du, Y.; Pascal, R. A.; Rubtsov, I. V. Unidirectional Coherent Energy Transport Via Conjugated Oligo(P-Phenylene) Chains. *J. Chem. Phys.* **2021**, *154*, 134304.
(71) Rubtsov, I. V.; Burin, A. L. Ballistic and Diffusive Vibrational Energy Transport in Molecules. *J. Chem. Phys.* **2019**, *150*, 020901.
(72) Rubtsova, N. I.; Rubtsov, I. V. Vibrational Energy Transport in Molecules Studied by Relaxation-Assisted Two-Dimensional Infrared Spectroscopy. *Annu. Rev. Phys. Chem.* **2015**, *66*, 717−738.
(73) Botan, V.; Backus, E. H. G.; Pfister, R.; Moretto, A.; Crisma, M.; Toniolo, C.; Nguyen, P. H.; Stock, G.; Hamm, P. Energy Transport in Peptide Helices. *Proc. Natl. Acad. Sci. U.S.A.* **2007**, *104*, 12749−12754.
(74) Deniz, E.; Valiño-Borau, L.; Löffler, J. G.; Eberl, K. B.; Gulzar, A.; Wolf, S.; Durkin, P. M.; Kaml, R.; Budisa, N.; Stock, G.; et al. Through Bonds or Contacts? Mapping Protein Vibrational Energy Transfer Using Non-Canonical Amino Acids. *Nat. Commun.* **2021**, *12*, 3284.
(75) Fujii, N.; Mizuno, M.; Ishikawa, H.; Mizutani, Y. Observing Vibrational Energy Flow in a Protein with the Spatial Resolution of a Single Amino Acid Residue. *J. Phys. Chem. Lett.* **2014**, *5*, 3269−3273.
(76) Buchenberg, S.; Leitner, D. M.; Stock, G. Scaling Rules for Vibrational Energy Transport in Globular Proteins. *J. Phys. Chem. Lett.* **2016**, *7*, 25−30.
(77) Suzuki, M.; Plakhotnik, T. The Challenge of Intracellular Temperature. *Biophys. Rev.* **2020**, *12*, 593−600.
(78) Sarkar, S.; Patrow, J. G.; Voegtle, M. J.; Pennathur, A. K.; Dawlaty, J. M. Electrodes as Polarizing Functional Groups: Correlation between Hammett Parameters and Electrochemical Polarization. *J. Phys. Chem. C* **2019**, *123*, 4926−4937.
(79) Zaragoza, J. P. T.; Offenbacher, A. R.; Hu, S.; Gee, C. L.; Firestein, Z. M.; Minnetian, N.; Deng, Z.; Fan, F.; Iavarone, A. T.; Klinman, J. P. Temporal and Spatial Resolution of Distal Protein Motions That Activate Hydrogen Tunneling in Soybean Lipoxygenase. *Proc. Natl. Acad. Sci. U.S.A.* **2023**, *120*, No. e2211630120.

https://doi.org/10.1021/acs.jpcc.4c01873
J. Phys. Chem. C XXXX, XXX, XXX−XXX